# Indoor Positioning of a Robotic Walking Assistant for Large Public Environments

Payam Nazemzadeh, *Student Member, IEEE*, Federico Moro, Daniele Fontanelli, *Member, IEEE*, David Macii, *Senior Member, IEEE*, and Luigi Palopoli

***Abstract*— Indoor localization and position tracking are essential to support applications and services for ambient-assisted living. While the problem of indoor localization is still open and already quite complex per se, in large public places, additional issues of cost, accuracy, and scalability arise. In this paper, the position estimation and tracking technique developed within the project devices for assisted living (DALi) is described, analyzed through simulations, and finally validated by means of a variety of experiments on the field. The goal of the DALi project is to design a robotic wheeled walker guiding people with psychomotor problems. Indeed, people with motor or cognitive impairments are often afraid of moving in large and crowded environments (e.g., because they could lose the sense of direction). In order to mitigate this problem, the position tracking approach described in this paper is based on multisensor data fusion and it is conceived to assure a good tradeoff between target accuracy, level of confidence, and deployment costs. Quite interestingly, the same approach could be used for indoor automated guided vehicles and robotics.**

***Index Terms*— Assistive devices, Kalman filtering, navigation, performance evaluation, position measurement, sensor fusion.**

## I. Introduction

ACCORDING to recent market forecasts and analyses, the worldwide turnover related to indoor navigation is expected to reach U.S. $2.6 billion in 2018 at a compounded annual growth rate of about 42% [1]. The range of potential applications of indoor localization is very large. One of the most interesting is the so-called *ambient-assisted living* (AAL), i.e., the application of information and communication technologies to the assistance of older adults or of people with impairments. In this field, most of the challenges come from the fragility of users and from their specific state of mind. In order to be applicable to AAL, a localization technology has to be robust, reliable, and, most importantly, acceptable to the user [2].

Manuscript received November 24, 2014; revised April 22, 2015; accepted April 23, 2015. Date of publication July 8, 2015; date of current version October 7, 2015. This work was supported by the European Union through the Seventh Framework Programme (FP7/2007-2013) under Grant ICT-2011-288917 within the Project entitled Devices for Assisted DALi. The Associate Editor coordinating the review process was Dr. Antonios Tsourdos.

P. Nazemzadeh, F. Moro, and L. Palopoli are with the Department of Information Engineering and Computer Science, University of Trento, Trento 38123, Italy (e-mail: payam.nazemzadeh@unitn.it; moro@disi.unitn.it; palopoli@disi.unitn.it).

D. Fontanelli and D. Macii are with the Department of Industrial Engineering, University of Trento, Trento 38123, Italy (e-mail: daniele.fontanelli@unitn.it; david.macii@unitn.it).

Color versions of one or more of the figures in this paper are available online at http://ieeexplore.ieee.org.

Digital Object Identifier 10.1109/TIM.2015.2437637

The project *devices for assisted living* (DALi) is an EU research initiative with the goal of developing a wheeled robotic assistant (called c-Walker) able to offer a concrete support to older adults in their navigation within complex indoor environments, such as shopping malls, railway stations, or airports. The c-Walker helps the user decide a route in the environment (e.g., to visit a sequence of desired locations), monitors the surroundings to detect possible anomalies or hazards, adapts the path to the changing conditions of the environment, and guides the user along the path using electromechanical brakes or haptic interfaces. Such tasks rely on accurate real-time position estimation, which is the specific topic of this paper.

Although the c-Walker is the outcome of a particular research project, the position tracking approach is applicable to a much larger class of service robots offering close assistance to their users. The main features of the proposed approach can be summarized as follows:

1) The wanted accuracy and the related level of confidence have to be good enough to enable fine-grained corrections and maneuver in confined spaces.
2) The cost of the device and the impact of the instrumentation in the environment should be reasonable both for common users and for the managers of the public space.
3) The form factor of the walker has to be acceptable in terms of size, weight, and invasiveness.
4) The proposed approach has to be scalable enough to allow the operation of several walkers at the same time.

All these requirements cannot be met using just a single localization technique. For instance, the positioning uncertainty of solutions based on radio signal strength intensity (RSSI) measurements and fingerprinting can be so large as a few meters, which is inadequate for the intended purpose [3]–[5].

Techniques based on round-trip time or time-of-arrival measurements of ultrawideband [6], [7], chirp spread spectrum [8]–[10], or ultrasonic signals [11], [12], even if accurate in line-of-sight (LOS) conditions, could be severely affected by fixed or moving obstacles, which are quite common in large public (and potentially crowded) environments. Moreover, the use of constantly active wireless links between the moving target and multiple fixed anchor nodes is hardly scalable and poses interference problems when multiple objects have to be tracked at the same time. Also, the measurement data collected by different nodes should be properly synchronized through an *ad-hoc* protocol, which may pose reliability and bandwidth issues [10], [13].

TABLE I
MAIN FEATURES OF VARIOUS POSITION TRACKING TECHNIQUES THAT INSPIRED THE APPROACH PROPOSED IN THIS PAPER

| Paper | Highlights | Pros | Cons |
|---|---|---|---|
| De Cecco [24] | - Odometry and Gyroscope<br>- Sensor data fusion depends on their uncertainties in different conditions of motion | - quite accurate after calibration | - Initialization required<br>- Bounded positioning uncertainty is not guaranteed in the long run |
| Park et al. [25] | - Passive RFIDs only<br>- At least one RFID must be read at every sampling time<br>- Position computed through an incremental trigonometric approach | - Absolute localization<br>- No other sensors are needed | - Large number of RFID tags<br>- Tested at very low speeds (12 cm/s) |
| Choi et al. [26] | - Fusion of active sensing and passive RFID reads<br>- Cameras on the ceiling to detect the position of the robot | - Absolute localization<br>- Accurate | - Large number of RFIDs<br>- It relies on external cameras<br>- Difficult to use in large rooms |
| Choi et al. [27] | - Combines global RFID-based positioning with local ultrasound-based distance measurements | - Absolute localization<br>- Very accurate | - Large number of RFID tags<br>- Position refinement difficult in spaces with moving obstacles. |
| Ahmad et al. [28] | - A special triangular multiloop-bridge reader antenna generates signals that are a function of tag location.<br>- Voltage signals are combined with information from database and with encoder data. | - Coarser RFID tag grid granularity<br>- High accuracy | - Maximum distance between RFID tags still too limited (about 130 cm) |
| Kulyukin et al. [29] | - Use of encoders<br>- Position correction through RFID mats | - Absolute localization<br>- Mats are easy to deploy and they can be sparse (due to the use of encoders) | - Works well in corridors, but not suitable in large rooms<br>- Unclear data fusion technique<br>- Compass not always suitable in indoor environments |
| Nazari et al. [30] | - Carpets of passive RFID<br>- Four RFID readers<br>- Position and orientation estimates based on simultaneous label detection | - Absolute localization<br>- Accurate<br>- Focus not only on positioning, but also on orientation estimates | - Large number of RFID tags<br>- Four RFID readers on the vehicle |

The use of wearable inertial measurement units (IMUs) installed either on shoes or on portable items for pedestrians [14]–[16], is possible in principle, but its efficacy for people with deambulation problems is questionable.

Finally, the position tracking techniques based exclusively on vision systems, even if precise, generally require powerful and expensive computational platforms [17], [18]. Moreover, the use of cameras is influenced by light conditions and may pose range, privacy, and scalability issues.

In order to tackle the manifold issues listed above, many researchers nowadays think that the best approaches for high performance and scalable indoor positioning should rely on multisensor data fusion [19], [20]. This is also the approach described in this paper. When a walking assistant, like the DALi's c-Walker, is used, odometry and gyroscopes data can be combined with *sporadic* external measurement results providing information on absolute position and direction of motion [21].

In the rest of this paper, first, in Section II, some related works are presented to emphasize the similarities and differences between the proposed technique and other solutions found in the literature. In Section III, the localization problem is formulated and the underlying system and measurement models are described. Such models partially derive from the results of preliminary studies reported in [22] and [23], but they have been improved in order to estimate and compensate the effect of possible left-/right-side mechanical asymmetries of the device. Section IV focused on the description of the chosen estimator. Section V reports some simulation results based on the data collected from real sensors. The purpose of the simulations is to analyze the behavior of the position tracking technique in different conditions to achieve a suboptimal tradeoff between performances and deployment costs. Such results are partially different from those reported in [21], because they are based on a better characterization of the sensors actually used in the development of the c-Walker. Section VI deals with a short description of the c-Walker prototype and includes the results of a variety of on-the-field experiments. Finally, Section VII concludes this paper.

## II. RELATED WORK

The results of the experimental activities reported in [31] confirmed that the accuracy of high-performance wireless ranging techniques is quite limited in non-LOS conditions. Thereby, a number of alternative approaches (in part borrowed from robotics) have been considered to fulfill the multifaceted requirements described in Section I. A list of the main research works that inspired the proposed approach, along with a short description of their advantages and disadvantages, is summarized in Table I.

First of all, since we deal with the localization of a wheeled device, a powerful resource for positioning is offered by odometry. However, as customary of dead reckoning techniques, odometry-based localization suffers from unbounded uncertainty growth and lack of initial observability. While position and orientation errors generally increase with a rate depending on both odometer resolution and accuracy, the estimation results can be considerably improved by fusing gyroscope and encoder data on the basis of their respective uncertainties in different conditions of motion [24].

Unfortunately, also in this case, there are no guarantees to keep the overall position uncertainty bounded. Moreover, the initial state of the system is still unobservable. To tackle these problems, an additional absolute localization technique is certainly needed. Given that no external wireless ranging solutions based on RSSI or ToF measurements proved to be accurate enough [31], the absolute position values can be obtained from a set of passive Radio Frequency Identification (RFID) tags. In fact, they are inexpensive, can be stuck on the floor at known locations, and, even if they have a quite limited range (in the order of a few tens of centimeters or less), they can be easily detected, regardless of the number of people and obstacles in the environment. Four good solutions of this kind are described in [25]–[28]. In [25], a fine-grained grid of passive RFID tags is used for robot navigation and trajectory reconstruction. No other sensors are employed. In [26], a similar approach is adopted, but an additional vision system is used to recognize the color patches placed on the top of different robots. In [27], a similar grid of RFID tags is used along with a set of ultrasonic sensors installed on the front side of a robot for position refinement through data fusion. A common characteristic of the solutions mentioned above is high accuracy, which, however, is paid in terms of RFID grid granularity. In fact, in all cases, the grids of tags are very dense (with distances between about 0.3 and 0.5 m), which is costly and impractical in very large environments. Moreover, the fixed external cameras in [26] pose privacy and scalability issues, while the on-board ultrasonic sensors (which refine position in the presence of fixed obstacles) could lead to unpredictable results in densely populated environments. In [28], the problem of RFID density is partially addressed by a special triangular multiloop-bridge reader antenna that generates voltage signals across a bridge circuit. Since such signals are a function of tag location, by combining them with both the information from a database and the data measured by the encoders of a wheeled device (e.g., a wheelchair), the position and the orientation of the device can be estimated with high accuracy and with a smaller number of RFID tags.

In this paper, our goal is not to maximize accuracy, but rather to assure a good compromise between accuracy, level of confidence, costs, and deployment complexity. A similar idea is also described in [29] that, to the best of our knowledge, is the solution that looks most similar to the technique presented in this paper. In [29], a smart walker instrumented with encoders, a compass, and an RFID reader corrects the odometry-based position by reading mats of RFID tags placed in strategic points of corridors (i.e., where people are supposed to come across with a high probability). However, the solution suffers from some drawbacks. First of all, the use of mats is not suitable for wide rooms where the user can potentially move in any direction. Second, the adopted sensor fusion algorithm is unclear. Apparently, the sensor measurement uncertainties are not used to support the estimation model, as instead it is done in this paper. Third, the problem of attitude estimation is addressed with a compass that, in our experience, can lead to very poor results in some indoor environments. In this respect, it is worth emphasizing that the long-term position uncertainty is crucially affected not only by the accuracy of the absolute localization system, but also by possible attitude or orientation errors. Even assuming that the coordinates of the moving target are perfectly adjusted when an RFID tag is detected, the position error may grow quickly if the estimated orientation is very different from the real one. This problem is not so visible when the RFID grid is dense, but it becomes significant when RFID grid granularity is coarse. In such cases, an additional sensing system able to measure the orientation of the walker in a global reference frame is needed, as it is confirmed by the analysis reported in [22]. This result is also consistent with the solution described in [30], where, in order to estimate the orientation of a mobile device over a carpet of RFID tags, four RFID readers are used to detect at least two tags at a time. Unfortunately, in our case, adding too many readers would make the walker bulky, fragile, and uncomfortable for the user. In addition, the distance between pairs of adjacent tags should be small enough to enable the detection of two tags at a time, thus making, again, the grid quite dense. Since compasses and magnetometers proved to be quite unreliable indoors, we decided to measure the walker's orientation by means of a low-cost front camera already available on the device for collision avoidance and trajectory planning. In particular, the camera is supposed to detect suitable markers (e.g., arrow-shaped adhesive stickers) deployed in the environment. Even if such markers could be aesthetically unpleasant in some contexts, the use of a standard and properly chosen type of markers makes the performance of the localization system more robust to changeable environmental conditions. Moreover, in spite of the typical problems that may arise when a vision system is employed in potentially crowded environments (e.g., due to obstacles), we think that cameras can still be very effective for the intended purpose, provided that the following conditions hold

1) The visual markers pointing toward a known direction are easy and unambiguous to detect.
2) The camera duty cycle is kept as low as possible (e.g., it is activated every few seconds).
3) The image processing algorithm is simple, robust, and computationally light.

## III. Problem Formulation

A qualitative overview of the framework underlying the proposed position estimation technique is shown in Fig. 1(a) and (b). In principle, the motion of a wheeled walker in a reference frame $\langle W \rangle = X_w \times Y_w \times Z_w$ can be described by the following basic kinematic system:

$$\dot{\mathbf{s}} = \begin{bmatrix} \dot{x} \\ \dot{y} \\ \dot{\theta} \end{bmatrix} = \begin{bmatrix} \upsilon \cos\theta - L\omega \sin\theta \\ \upsilon \sin\theta + L\omega \cos\theta \\ \omega \end{bmatrix} \tag{1}$$

$$\mathbf{o} = \mathbf{s} \tag{2}$$

where $\mathbf{s} = [x, y, \theta]^T$ is the vector of the state variables, $\upsilon$ is the forward velocity of the walker along the direction of motion, $\omega$ is its angular velocity, $L$ is a constant representing the minimum distance between the midpoints of the rear and front wheels, respectively, and $\mathbf{o}$ is the output vector of the system. Note that $(x, y)$ in Fig. 1(a) are the Cartesian

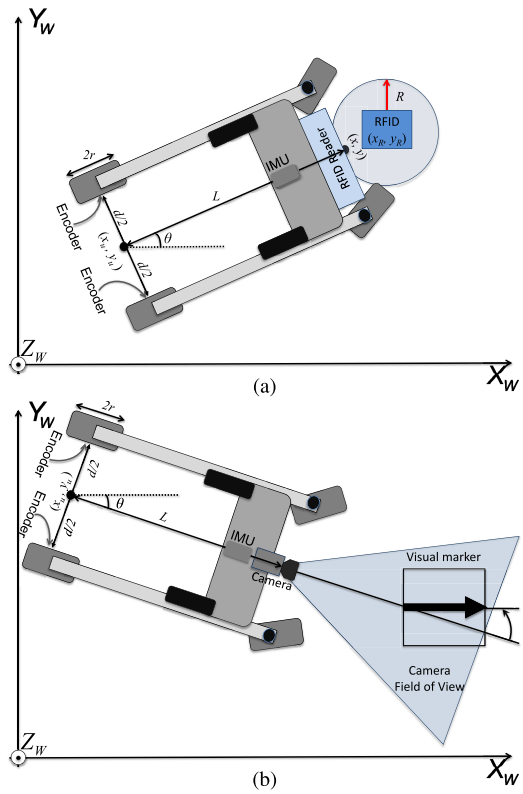


Fig. 1. Qualitative overview of the walker's position estimation problem, with a special emphasis on (a) RFID tag detection and (b) visual marker recognition.

coordinates of the midpoint of the front wheel axle on plane $X_w \times Y_w$, while $\theta$ is the walker's orientation angle. This angle is defined by the longitudinal axis of symmetry of the walker with respect to axis $X_w$, as shown in Fig. 1(b). Since the walker acts as a unicycle-like vehicle, the forward and angular velocities, $v$ and $\omega$, can be regarded as functions of the rear wheel velocities, i.e., $v = r/2(\omega_r + \omega_l)$ and $\omega = r/d(\omega_r - \omega_l)$, where $\omega_r$ and $\omega_l$ are the angular velocities of the right and left wheels, respectively, $r$ is the wheel radius, and $d$ is the rear axle length. Ideally, once the initial position and orientation of the walker are known, measuring $v$ and $\omega$ over time would be sufficient to reconstruct its position. However, both random and systematic measurement contributions tend to accumulate, thus leading to poor accuracy in the long run. Therefore, in order to mitigate this problem, such contributions should be properly included in the system model and they should also be taken into account by the chosen estimator. Observe that the state variables in $\mathbf{s}$ refer to the midpoint of the front wheels, which is the position where both the camera and the RFID are installed. However, in practice, we are mainly interested in the position $(x_u, y_u)$ of the human pushing the walker. Assuming that his/her centroid is reasonably aligned with the midpoint of the rear wheels, the following transformation holds:

$$\begin{bmatrix} x_u \\ y_u \end{bmatrix} = \begin{bmatrix} x - L\cos\theta \\ y - L\sin\theta \end{bmatrix}. \tag{3}$$

Therefore, the localization problem described in this paper has two complementary objectives:

1) estimating the coordinates $(x_u, y_u)$ of the human with a root mean square (RMS) Euclidean error no larger than $\eta_p$ with at least $\alpha_p$ probability;
2) estimating the walker's orientation angle $\theta$ with an RMS error no larger than $\eta_o$ with at least $\alpha_o$ probability.

### A. System Description

In nonideal conditions, the system model should explicitly take those phenomena into account (such as undetected encoder pulses, slight differences in wheels radius, mechanical asymmetries, and noise), which make position and orientation uncertainty grow indefinitely. As a result, the continuous-time system model (1) can be changed as follows:

$$\dot{\mathbf{s}}' = \begin{bmatrix} \dot{x} \\ \dot{y} \\ \dot{\theta} \\ \dot{\mu} \\ \dot{\delta} \end{bmatrix} = \begin{bmatrix} (1+\mu)v\cos\theta - L\omega(1+\delta)\sin\theta \\ (1+\mu)v\sin\theta + L\omega(1+\delta)\cos\theta \\ \omega(1+\delta) \\ \gamma_\mu \\ \gamma_\delta \end{bmatrix} \tag{4}$$

where the state vector $\mathbf{s}'$ comprises not only $\mathbf{s}$, but also the additional variables $\mu$ and $\delta$. These represent the relative systematic offsets between the forward and angular velocity values at a given time and the respective odometry-based values. Observe that the time evolution of $\mu$ and $\delta$ relies on functions $\gamma_\mu$ and $\gamma_\delta$, which depend on specific features of the system considered and should be determined through a proper experimental characterization. For instance, if in (5) $\gamma_\mu = \gamma_\delta = 0$, then $\mu$ and $\delta$ are just constant coefficients. System (4) can be conveniently expressed as a function of the angular velocity of the rear wheels

$$\dot{\mathbf{s}}' = \mathbf{g}(\mathbf{s}')\boldsymbol{\Omega} + H\boldsymbol{\Gamma} \tag{5}$$

where $\boldsymbol{\Omega} = [\omega_r, \omega_l]^T$, $\boldsymbol{\Gamma} = [\gamma_\mu, \gamma_\delta]^T$

$$\mathbf{g}(\mathbf{s}') = \begin{bmatrix} c_\mu\cos\theta - Lc_\delta\sin\theta & c_\mu\cos\theta + Lc_\delta\sin\theta \\ c_\mu\sin\theta + Lc_\delta\cos\theta & c_\mu\sin\theta - Lc_\delta\cos\theta \\ c_\delta & -c_\delta \\ 0 & 0 \\ 0 & 0 \end{bmatrix}.$$

$c_\mu = \frac{r}{2}(1+\mu)$, $c_\delta = \frac{r}{d}(1+\delta)$, $H = [\mathbf{0}_{2,3}, I_2]^T$, $\mathbf{0}_{m,n}$ is a $m \times n$ matrix filled with zeros, and $I_n$ is the identity matrix of dimension $n$. Note that $\mathbf{g}(\cdot)$ in (5) is a nonlinear vector function of the state. If (5) is discretized with sampling period $T_s$, the corresponding discrete-time system becomes

$$\mathbf{s}'_{k+1} = \mathbf{s}'_k + \mathbf{g}(\mathbf{s}'_k)\boldsymbol{\Delta\Phi}_k + T_s H\boldsymbol{\Gamma} \tag{6}$$

where $\mathbf{s}'_k$ denotes the state vector at time $kT_s$ and $\boldsymbol{\Delta\Phi}_k = \boldsymbol{\Omega}_k T_s = [\Delta\Phi_{r_k}, \Delta\Phi_{l_k}]^T$ is the vector of the angle displacements of the left and right wheels between $kT_s$ and $(k+1)T_s$. Of course, the measured values of $\boldsymbol{\Delta\Phi}_k$ are generally affected by zero-mean random fluctuations $\boldsymbol{\epsilon}_k = [\epsilon_{r_k}, \epsilon_{l_k}]^T$ due to, for instance, vibrations, electronic noise, and finite encoder resolution. Such random uncertainty contributions can

be reasonably assumed to be independent. Therefore, (6) can be changed as follows:

$$\begin{aligned}\mathbf{s}'_{k+1} &= \mathbf{s}'_k + \mathbf{g}(\mathbf{s}'_k)(\boldsymbol{\Delta\Phi}_k + \boldsymbol{\epsilon}_k) + T_s H \boldsymbol{\Gamma} \\ &= \mathbf{s}'_k + \mathbf{g}(\mathbf{s}'_k)\widehat{\boldsymbol{\Delta\Phi}_k} + T_s H \boldsymbol{\Gamma} \end{aligned} \tag{7}$$

where $\widehat{\boldsymbol{\Delta\Phi}_k} = [\widehat{\Delta\Phi_{r_k}}, \widehat{\Delta\Phi_{l_k}}]^T$ is the vector of the angle displacements measured between time $kT_s$ and time $(k+1)T_s$.

### *B. Measurement Model Description*

As shown in (2), the output vector $\mathbf{o}_k$ of the system in principle should be equal to $\mathbf{s}_k$. However, in practice, not all output quantities can be measured at every sampling time.

As explained in Section II, the c-Walker is equipped with two encoders, a short-range RFID reader, a gyroscope, and a front camera. While encoders and gyroscope can collect data at a rate equal to $1/T_s$, the RFID reader and the camera can detect a tag or a marker only if they are within their respective reading range. The identification (ID) code of each tag corresponds to known coordinates in $\langle W \rangle$, as shown in Fig. 1(a). However, no information about orientation is provided, since this generally cannot be measured through a single tag detection, unless special antennas are used [28].

To solve this problem, the orientation angle is estimated using both the gyroscope available inside an inertial measurement platform (IMU), and the orientation data extracted from the images collected from the camera, as shown in Fig. 1(b). In fact, the relative orientation angle with respect to a given initial value could be easily obtained by integrating the angular velocity of the walker around axis $Z_w$. However, the initial orientation is not observable and, in addition, the noise of the gyroscope also accumulates, thus potentially causing large random walk fluctuations in the long run. This problem could be addressed through a plain monodimensional Kalman filter. The process noise of this filter can be assumed to have zero-mean and standard deviation $\sigma_{\omega_k} = a|\omega_{z_k}| + b$, where $\omega_{z_k}$ is the angular velocity measured by the gyroscope at time $kT_s$, while $a$ and $b$ are the constant coefficients. This nonstationary model results from experimental evidence. In fact, several tests performed on real gyroscopes using an orbital rotator Stuart SB3 at various speeds in the range 2–40 RPM showed that the standard deviation of the gyroscope's noise tends to grow linearly with the rotational speed. Thus, the values of coefficients $a$ and $b$ can be easily estimated through a linear fitting.

Using this model, the prediction equations of the Kalman filter can be concisely written as follows:

$$\bar{\theta}^+_{k+1} = \bar{\theta}_k + T_s\omega_{z_k}, \quad \sigma^{2^+}_{\theta_{k+1}} = \sigma^2_{\theta_k} + T_s^2\sigma^2_{\omega_k} \tag{8}$$

where $\cdot^+$ denotes the prediction, $\bar{\theta}_k$ is the angle estimated at time $kT_s$ (not to be confused with the homonymous state variable in $\mathbf{s}'_k$), and $\sigma^2_{\theta_k}$ is its variance. If no visual markers are in the field of view of the camera (as it is supposed to happen most times), then the Kalman filter is updated just using the predicted values, i.e., $\bar{\theta}_{k+1} = \bar{\theta}^+_{k+1}$ and $\sigma^2_{\theta_{k+1}} = \sigma^{2^+}_{\theta_{k+1}}$. If instead a visual marker is detected, the corresponding frame is turned into a top-view image through the so-called inverse perspective mapping (IPM) [32]. Since the features of interest of the detected marker (e.g., an arrow) is associated with the direction of axis $X_w$, the orientation of the walker with respect to $X_w$ is given by the angle between the line bisecting longitudinally the top-view image and the direction of the detected marker, as shown in Fig. 1(b). As a result, the orientation angle and its variance are updated as follows:

$$\bar{\theta}_{k+1} = \bar{\theta}^+_{k+1} + \frac{\sigma^{2^+}_{\theta_{k+1}}\left(\theta^c_{k+1} - \bar{\theta}_{k+1}\right)}{\sigma^{2^+}_{\theta_{k+1}} + \sigma^2_{\theta^c_{k+1}}} \tag{9}$$

$$\sigma^2_{\bar{\theta}_{k+1}} = \frac{\sigma^2_{\theta^c_{k+1}}\sigma^{2^+}_{\theta_{k+1}}}{\sigma^{2^+}_{\theta_{k+1}} + \sigma^2_{\theta^c_{k+1}}} \tag{10}$$

where $\theta^c_{k+1}$ and $\sigma^2_{\theta^c_{k+1}}$ denote the angle measured by the camera-based system and its variance at time $(k+1)T_s$, respectively.

In conclusion, the overall measurement model is

$$\mathbf{o}_k = C_k\mathbf{s}'_k + \boldsymbol{\zeta}_k \tag{11}$$

where the output vector $\mathbf{o}_k$, the output matrix $C_k$, and the vector $\boldsymbol{\zeta}_k$ of the measurement uncertainty contributions depend on what sensor data are actually available at time $kT_s$. Evidently, the elements of $\boldsymbol{\zeta}_k$ can be regarded as independent, as they are completely related to different sensors. Thus, the covariance matrix $D_k$ associated with $\boldsymbol{\zeta}_k$ is diagonal.

Ultimately, two scenarios are possible:

1) If no RFID tags are detected, then $C_k = [0\ 0\ 1\ 0\ 0]$ and $D_k = \sigma^2_{\theta_k}$. This is the variance of the orientation angle estimated through the Kalman filter described above.
2) If instead an RFID tag is detected, then

$$C_k = \begin{bmatrix} 1 & 0 & 0 & 0 & 0 \\ 0 & 1 & 0 & 0 & 0 \\ 0 & 0 & 1 & 0 & 0 \end{bmatrix}, \quad D_k = \begin{bmatrix} \sigma^2_{x_k} & 0 & 0 \\ 0 & \sigma^2_{y_k} & 0 \\ 0 & 0 & \sigma^2_{\theta_k} \end{bmatrix} \tag{12}$$

where $\sigma^2_{\theta_k}$ is, again, the variance of the angle estimated with the previous Kalman filter, while $\sigma^2_{x_k}$ and $\sigma^2_{y_k}$ are the variances of the offsets between the nominal coordinates of the detected tag and the actual coordinates of the walker along axes $X_w$ and $Y_w$. Assuming, to a first approximation, that the probability of reading a tag is constant within the circle centered in the tag itself and with radius $R$ equal to the maximum nominal range of the RFID reader, then the uncertainty contributions associated with coordinates $x$ and $y$ are uncorrelated and $\sigma^2_{x_k} = \sigma^2_{y_k} = R^2/4$ [23].

## IV. Walker Position Estimation and Tracking

In general, the state of a nonlinear system can be efficiently estimated by an extended Kalman filter (EKF) under the assumptions that: 1) the system and output model nonlinearities are quite smooth and 2) the various uncertainty contributions are normally distributed with a zero mean. Since the potential nonzero relative velocity offsets modeling encoder imperfections are now explicitly included in the system, possible harmful biases can be introduced only by

the RFID-based position measurements and/or by the camera-based or gyroscope-based angular measurements. However, in the domain of all possible trajectories, the mean values of such uncertainty contributions can be reasonably assumed to be zero. Also, their distribution generally exhibits a quite Gaussian behavior [23], with the only exception of the RFID tag detection mechanism that, as explained in Section III-B, can be more realistically described by a uniform probability density function with a quasi-circular symmetry around a detected tag. Note that this issue does not affect the validity of the EKF. Also, lack of stationarity is not a problem for the EKF, as it works properly even when the process and measurement noises change over time, as it happens in the case considered.

Starting from these assumptions and with reference to the discrete-time system (6), the predicted state estimate at time $(k+1)T_s$ results from [33]

$$\hat{\mathbf{s}}'^{+}_{k+1} = \hat{\mathbf{s}}'_k + g(\hat{\mathbf{s}}'_k)\widehat{\mathbf{\Delta\Phi}}_k \tag{13}$$

where $\hat{\mathbf{s}}'_k = [\hat{x}_k, \hat{y}_k, \hat{\theta}_k, \hat{\mu}_k, \hat{\delta}_k]^T$ is the state estimated at time $kT_s$. Observe that $\mathbf{\Gamma}_k$ is omitted in (13), because the mean value of this term is zero. The covariance matrix associated with the predicted state simply results from the linearization of (6)

$$P^+_{k+1} = F_k P_k F_k^T + G_k Q_k G_k^T + H U_k H^T \tag{14}$$

where $P_k$, $Q_k$, and $U_k$ are the covariance matrices associated with the estimated state, to $\boldsymbol{\epsilon}_k$ and to $\mathbf{\Gamma}_k$, respectively; and $F_k$ is the Jacobian of the state-space model with respect to $\mathbf{s}'_k$ at $[\hat{\mathbf{s}}'_k, \widehat{\mathbf{\Delta\Phi}}_k]$

$$F_k = \left.\frac{\partial\left[\mathbf{s}'_k + \mathbf{g}(\mathbf{s}'_k)\mathbf{\Delta\Phi}_k\right]}{\partial \mathbf{s}'_k}\right|_{\left[\hat{\mathbf{s}}'_k, \widehat{\mathbf{\Delta\Phi}}_k\right]} = \begin{bmatrix} 1 & 0 & f_1 & f_2 & f_3 \\ 0 & 1 & f_4 & f_5 & f_6 \\ 0 & 0 & 1 & 0 & f_7 \\ 0 & 0 & 0 & 1 & 0 \\ 0 & 0 & 0 & 0 & 1 \end{bmatrix} \tag{15}$$

with

$$\begin{aligned}
f_1 &= -c_{\widehat{\mu}_k} \sin\hat{\theta}_k(\widehat{\Delta\Phi}_{r_k} + \widehat{\Delta\Phi}_{l_k}) - Lc_{\widehat{\delta}_k} \cos\hat{\theta}_k(\widehat{\Delta\Phi}_{r_k} - \widehat{\Delta\Phi}_{l_k}) \\
f_2 &= \frac{r}{2}\cos\hat{\theta}_k(\widehat{\Delta\Phi}_{r_k} + \widehat{\Delta\Phi}_{l_k}) \\
f_3 &= -L\frac{r}{d}\sin\hat{\theta}_k(\widehat{\Delta\Phi}_{r_k} - \widehat{\Delta\Phi}_{l_k}) \\
f_4 &= c_{\widehat{\mu}_k} \cos\hat{\theta}_k(\widehat{\Delta\Phi}_{r_k} + \widehat{\Delta\Phi}_{l_k}) - Lc_{\widehat{\delta}_k} \sin\hat{\theta}_k(\widehat{\Delta\Phi}_{r_k} - \widehat{\Delta\Phi}_{l_k}) \\
f_5 &= \frac{r}{2}\sin\hat{\theta}_k(\widehat{\Delta\Phi}_{r_k} + \widehat{\Delta\Phi}_{l_k}) \\
f_6 &= L\frac{r}{d}\cos\hat{\theta}_k(\widehat{\Delta\Phi}_{r_k} - \widehat{\Delta\Phi}_{l_k}) \\
f_7 &= \frac{r}{d}(\widehat{\Delta\Phi}_{r_k} - \widehat{\Delta\Phi}_{l_k})
\end{aligned}$$

and, finally, $G_k = \mathbf{g}(\hat{\mathbf{s}}'_k)$ since the model is linear with respect to the inputs.

Consider that $U_k$ in the following will be neglected as the drift coefficients in $\mathbf{\Gamma}_k$ are assumed to be purely deterministic. On the contrary, $Q_k$ depends on the performances of the chosen encoders. Since they are nominally identical, but independent, their uncertainty contributions can be assumed to be independent as well. Therefore, $Q_k$ is a $2 \times 2$ diagonal matrix with $\sigma^2_{r_k}$ and $\sigma^2_{l_k}$ on the main diagonal. It is worth emphasizing that, to a first approximation, the standard deviation of the angular displacements measured by the right- and left-wheel encoder can be reasonably assumed to linearly grow with their respective angular velocities, i.e., $\sigma_{r_k} = \sigma_e \omega_{r_k} T_s$ and $\sigma_{l_k} = \sigma_e \omega_{l_k} T_s$.

The Kalman filter gain is then given by [33]

$$K_{k+1} = P^+_{k+1} C^T_{k+1}\left(C_{k+1} P^+_{k+1} C^T_{k+1} + D_{k+1}\right)^{-1} \tag{16}$$

where $C_{k+1}$ and $D_{k+1}$ depend on the measurement data available at time $(k+1)T_s$, as explained in Section III-B. Thus, the Kalman gain (16) and the set of measurement data $\mathbf{o}_{k+1}$ collected at time $(k+1)T_s$ are used to update the system state estimate and the corresponding covariance matrix

$$\begin{aligned}
\hat{\mathbf{s}}'_{k+1} &= \hat{\mathbf{s}}'^{+}_{k+1} + K_{k+1}\left(\mathbf{o}_{k+1} - C_{k+1}\hat{\mathbf{s}}'^{+}_{k+1}\right) \\
P_{k+1} &= (I_3 - K_{k+1}C_{k+1})P^+_{k+1}.
\end{aligned} \tag{17}$$

It is worth reminding that the position of the user at time $kT_s$ is not given by $(\hat{x}_k, \hat{y}_k)$, but rather by $(\hat{x}_{u_k}, \hat{y}_{u_k})$ which is obtained by replacing $(\hat{x}_k, \hat{y}_k, \hat{\theta}_k)$ into (3).

## V. Simulation-Based Analysis

The accuracy of the dynamic estimator described in Section IV has been evaluated through several Monte Carlo simulations over hundreds of random paths of various lengths. No obstacles or walls (except for the perimeter fence) have been used to constrain the generated paths. Therefore, the performances of the algorithm have been tested in all directions and at different linear and angular velocities, i.e., for $v \in [0, 2]$ m/s and $\omega \in [-1, 1]$ rad/s. These intervals are indeed compatible with a typical human behavior. The values of the simulation parameters of encoders, gyroscope, RFID reader, and camera have been obtained either from data sheets or from a preliminary characterization of the sensors and devices actually used in the development of the c-Walker prototype [23]. The list of such devices is reported in Section VI. For the sake of completeness, the values of the simulation parameters are listed as follows:

1) encoder and gyroscope sampling period: $T_s = 4$ ms;
2) standard uncertainty of encoder angular increments: $\sigma_{r_k} = 0.066\Delta\Phi_{r_k} + 0.005$ and $\sigma_{l_k} = 0.066\Delta\Phi_{l_k} + 0.005$;
3) standard deviation of the angular velocity values measured by the gyroscope (normally distributed): $\sigma_{\omega_{z_k}} = 0.15|\omega_{z_k}| + 0.08$ rad/s;
4) standard deviation of the camera-based orientation measurements (normally distributed): $\sigma_{\theta^c_k} \approx 30$ mrad, with a maximum marker detection range of 1.2 m and a maximum forward angle view of 0.7 rad;
5) RFID tag detection radius (circular symmetry): $R = 15$ cm with a tolerance of $\pm 1$ cm;
6) forward velocity drift coefficient: $\mu \approx 0.015$;
7) angular velocity drift coefficient: $\delta \approx -0.01$.

The elements of the covariance matrix of the estimated state are initialized to unrealistically large values since no *a priori* information is available at time 0.

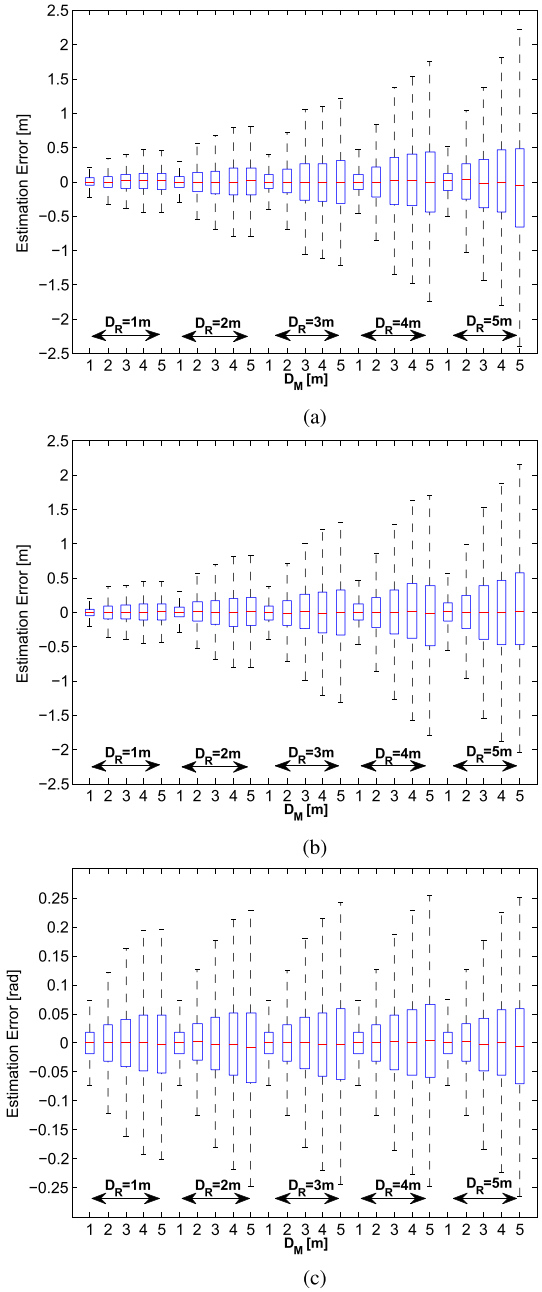


Fig. 2. Box-and-whisker plots of (a) $x_u$, (b) $y_u$, and (c) $\theta$ estimation errors in 200 random trajectories, assuming to use the grids of RFID tags and visual markers of different granularity [i.e., 25 pairs of $(D_R, D_M)$ values with $D_R$ and $D_M \in \{1, 2, 3, 4, 5\}$ m].

In the first set of simulations, 200 random trajectories of 180 s each have been generated in a large open room, assuming to use two independent grids of equally spaced tags and markers of different granularities. If $D_R$ and $D_M$ denote the distances between pairs of adjacent RFID tags and markers, respectively, the state estimation errors for each trajectory have been computed in 25 different configurations, obtained with both $D_R$ and $D_M \in \{1, 2, 3, 4, 5\}$ m. Fig. 2(a)–(c) shows the box-and-whisker plots of the $x_u$, $y_u$, and $\theta$ estimation errors for different pairs of $D_R$ and $D_M$. Observe that, with the chosen values of the simulation parameters, the accuracy of both position and orientation estimation degrades quite quickly as the distance between tags or markers grows. Consider also that for $D_M = 1$ m, a visual marker is almost always in the reading range of the camera. Therefore, the average update rate is high, thus drastically improving the performances. When either $D_R$ or $D_M$ ranges between 1 and 3 m, the $x_u$ or $y_u$ estimation errors are generally within $\pm 50$ cm, with a few outliers in the order of $\pm 1$ m. In addition, in the same conditions, the orientation estimation errors are generally within $\pm 0.15$ rad. Further simulation results (not shown for the sake of brevity, but qualitatively quite similar to those reported in [21]) confirm that including in the model the drift coefficients of forward and angular velocity (i.e., variables $\mu$ and $\delta$) provides better accuracy than using an EKF with just three state variables (i.e., $x$, $y$, and $\theta$ only). This result is expected since, in the latter case, the systematic velocity-dependent uncertainty contributions due to walker asymmetries and encoders differences are not estimated and compensated grids.

A crucial point that has to be addressed in view of deploying the proposed solution in a real environment is the optimal selection of the values of $D_R$ and $D_M$. In theory, $D_R$ and $D_M$ should be chosen in such a way that the total number of tags and markers in the environment is minimum and the wanted position and orientation accuracy boundaries are met, as specified in Section III. Unfortunately, an analytical formalization and a solution to this optimization problem are challenging, and they deserve a study on its own, which is out of the scope of this paper. RFID tags and visual markers have a crossed random effect on EKF updates. The RFID tags are conceived to adjust the position, but they also partially contribute to correct the orientation angle through the Kalman gain (16). Dually, even if the visual markers mainly adjust the estimated orientation angles, they also indirectly affect the position values. Thus, the solution to the placement optimization problem depends not only on the granularity of grids of tags and markers, taken individually, but also on their combination. The problem is further complicated by the need to define a realistic and tractable stochastic model describing user's trajectories.

In order to find a solution, at least suboptimal, to this challenging problem, a numerical approach based on Monte Carlo simulations has been adopted. The proposed procedure consists of the following two steps.

1) At first we can find the maximum values of $D_R$ and $D_M$ (denoted as $D_{R_p}$ and $D_{M_p}$, respectively) for which the RMS position error (expressed in terms of Euclidean distance from the actual position) is smaller than or equal to $\eta_p$ with (at least) $\alpha_p$ probability.
2) Afterwards, a dual approach can be used to determine the maximum values of $D_R$ and $D_M$ (denoted as $D_{R_o}$ and $D_{M_o}$, respectively) for which the RMS orientation error is smaller than or equal to $\eta_o$ with (at least) $\alpha_o$ probability.

Eventually, the suboptimal values of the distances between pairs of markers and tags can be obtained by simply choosing the more conservative solution in either, i.e.,

$$D_R^* = \min\{D_{R_p}, D_{R_o}\} \text{ and } D_M^* = \min\{D_{M_p}, D_{M_o}\}. \quad (18)$$

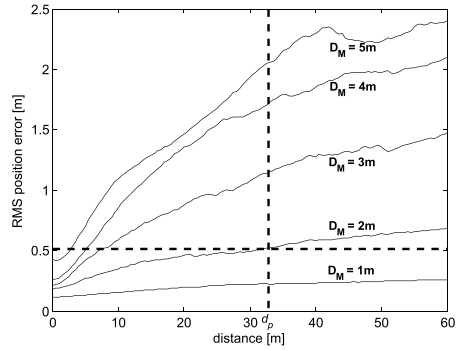


(a)

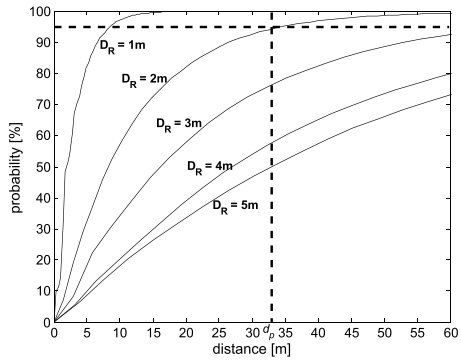


(b)

Fig. 3. (a) RMS Euclidean distances between the estimated and actual positions as a function of the traveled distance when the RFID reader is disabled and $D_M \in \{1, 2, 3, 4, 5\}$ m. (b) Cumulative distribution functions associated with the probability to meet an RFID tag as a function of the traveled distance from a previous tag when $D_R \in \{1, 2, 3, 4, 5\}$ m.

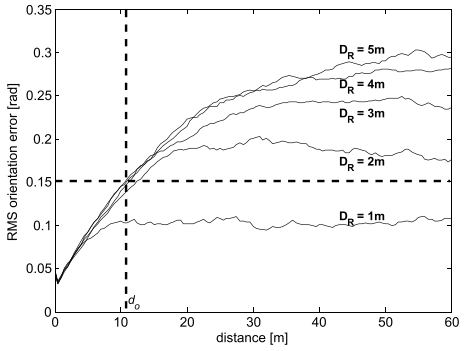


(a)

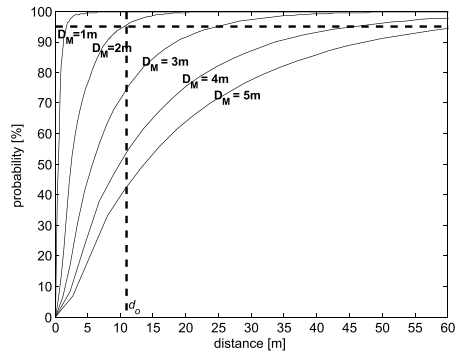


(b)

Fig. 4. (a) RMS values of the orientation errors as a function of the traveled distance when the camera is disabled and $D_R \in \{1, 2, 3, 4, 5\}$ m. (b) Cumulative distribution functions associated with the probability to meet a visual marker as a function of the traveled distance from a previous marker when $D_M \in \{1, 2, 3, 4, 5\}$ m.

To address the first problem, assuming to disable the RFID reader only, the RMS values of the Euclidean distances between the estimated and actual positions have been calculated as a function of the path length over 500 random routes for $D_M \in \{1, 2, 3, 4, 5\}$ m. The respective RMS position error curves are shown in Fig. 3(a). At the same time, the cumulative distribution functions associated with the probability for the walker to meet an RFID tag as a function of the traveled distance from a previous tag are plotted in Fig. 3(b) for $D_R \in \{1, 2, 3, 4, 5\}$ m. Fig. 3(a) allows to determine $D_{M_p}$ and the distance $d_p$ that the walker can cover prior to exceeding threshold $\eta_p$. Once $d_p$ and $D_{M_p}$ are known, the value of $D_{R_p}$ is given by the cumulative distribution function for which the $\alpha_p$-percentile of detecting an RFID tag is equal to $d_p$. For instance, in Fig. 3(a) and (b), the horizontal dashed lines refer to $\eta_p = 50$ cm and $\alpha_p = 95\%$, respectively. Such values meet the requirements of the DALi project. In particular, if $\eta_p = 50$ cm and $D_{M_p} \approx 2$ m, it results from Fig. 3(a) (vertical dashed line) that $d_p \approx 33$ m. Thus, it immediately follows from Fig. 3(b) that, when $d_p \approx 33$ m, then $D_{R_p} \approx 2$ m.

A dual record of Monte Carlo simulations has been performed to build the RMS orientation error curves as a function of the path length for $D_R \in \{1, 2, 3, 4, 5\}$ m, assuming that the front camera is disabled. Such curves are shown in Fig. 4(a). Also, the cumulative distribution functions associated with the probability to meet a visual marker as a function of the traveled distance from a previous marker are plotted in Fig. 4(b) for $D_M \in \{1, 2, 3, 4, 5\}$. Observe that these curves differ from those shown in Fig. 3(b), because the detection range of RFID reader and camera is also different. The approach to estimate $D_{R_o}$ and $D_{M_o}$ is dual to the one described above. At first, the distance $d_o$ that the walker can cover prior to exceeding $\eta_o$ and the corresponding value of $D_{R_o}$ can be obtained from Fig. 4(a). Then, $D_{M_o}$ can be estimated from Fig. 4(b) by finding the largest value of $D_M$ for which the probability of meeting a marker after $d_o$ meters is at least $\alpha_o$. If, for instance, $\eta_o = 0.15$ rad and $\alpha_o = 95\%$ (also these values are compliant with the requirements of the DALi project) Fig. 4(a) shows that $d_o \approx 11$ m when $D_{R_o} \approx 5$ m. Therefore, it results from Fig. 4(b) that for the same $d_o$ value $D_{M_o} \approx 2$ m. Ultimately, it follows from (18) that the distance between pairs of adjacent RFID tags and markers should be so conservatively set equal to $D_R^* \approx D_M^* \approx 2$ m.

## VI. Implementation and Experimental Results

The position tracking algorithm described in Section III was tested on a real c-Walker prototype (Fig. 5) in the laboratories of the Department of Industrial Engineering of the University of Trento. The data from the CUI Inc. AMT10X encoders installed on the rear wheels as well as the samples from an Invensense IMU-3000 gyroscope on-board of the IMU already used in [16] are transferred to a Beaglebone embedded platform via CAN bus at 250 Hz. The Beaglebone is equipped with an AM335× ARM Cortex A8 processor

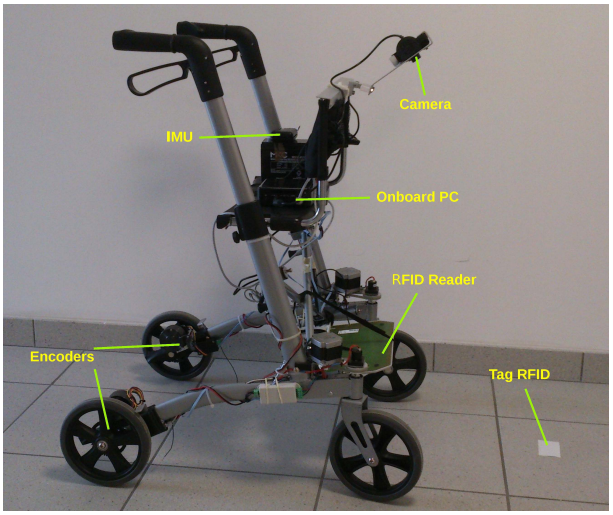


Fig. 5. c-Walker prototype.

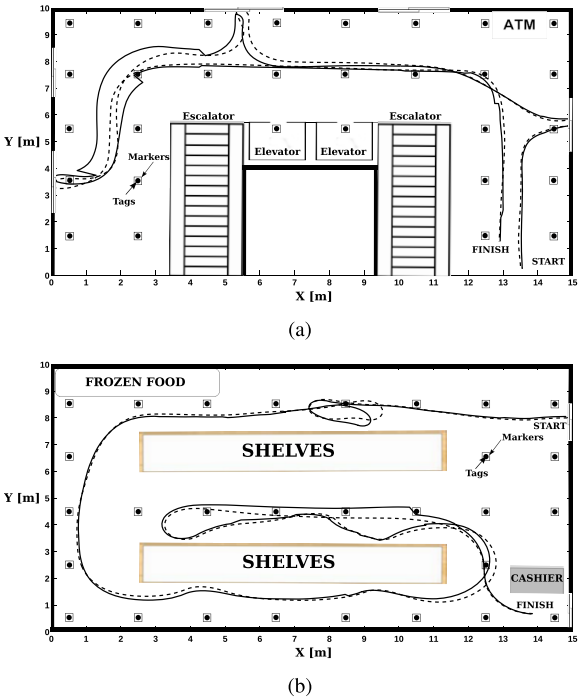


Fig. 6. Two examples of estimated trajectories (solid lines) in two different scenarios: (a) hall of a shopping mall and (b) some aisles of a supermarket. The dashed lines are the actual routes of the c-Walker reconstructed from the laser scanner data after smoothing. The uncertainty of such trajectories is in the order of a few centimeters.

running at 720 MHz and 256 MB of DDR2 RAM. The operating system on-board of the Beaglebone is a Debian Linux distribution with kernel v.3.2 patched with the RT-Preempt package to improve determinism and real-time performance. The Beaglebone also collects the data from a Feig ISC.MR101 RFID reader through a USB connection. Data acquisition and processing are implemented in C language. All the components above are powered by a 12 V 7-Ah lead-acid battery. The preprocessed measurement results, aligned on the same timescale, are transferred via Ethernet to a laptop PC equipped with a 2.26-GHz Intel Core 2 Duo processor and 2 GB of DDR2 RAM. The operating system running on the PC is a standard Ubuntu Linux. A PSeye USB webcam is directly linked to the PC and it is activated with a resolution of $640 \times 480$ pixels at a rate of just 10 Hz, to reduce both communication bandwidth requirements and computational burden. The program for visual marker recognition is implemented in C++ using the primitives of the well-known OpenCV library. The position estimation and tracking algorithm is instead implemented in C. For testing and debugging reasons, at the moment both this algorithm and the software application visualizing the motion of the c-Walker on a map run on the laptop. However, in a future version of the c-Walker, they will be ported to a high-performance embedded system with a smaller form factor.

The area chosen for the experimental activities is a large room of about 300 $m^2$ in the basement of the Department of Industrial Engineering. The room was instrumented with RFID tags and markers put on the floor. In all experiments, $D_R^* \approx D_M^* \approx 2$ m in accordance with the simulation-based results described in Section V. All visual markers were directed as axis $X_w$. About 50 experiments of a different duration were conducted with the c-Walker pushed at various speeds and along different routes, both throughout the empty room and with some obstacles on the way to emulate realistic scenarios. In order to evaluate the accuracy of the position tracking technique, a laser scanner SICK S300 Expert was placed in the origin of reference frame $\langle W \rangle$ (i.e., in one corner of the room) to measure the coordinates of the user along each route in real time. The laser scanner has an angular resolution of 0.5°, a maximum scanning angle of up to 270° (but this was limited to 90° to increase the scanning rate), and a maximum reading range of about 30 m. According to the instrument specifications, the ranging measurement accuracy depends on the size of the object and degrades as the distance from the target grows. Thus, to keep the positioning uncertainty of the laser-based system at least one order of magnitude smaller than the uncertainty of the system under test (i.e., in the order of a few centimeters), most of the experiments were conducted over just 150 $m^2$ of the available space. Also, the scanner was put on top of a 2-m-high shelf to detect just the head of the user instead of the whole c-Walker. In this way, the cluster of points collected from the scanner at a given time is quite concentrated around $(x_u, y_u)$ and finding the position of the centroid of the cluster is simpler. The coordinates of such a centroid provide a reasonably accurate estimate of the position of the user.

Fig. 6(a) and (b) shows the results of two experiments in two possible scenarios recreated artificially in the room, i.e., the entrance hall of a shopping mall (*scenario a*) and the aisles of a supermarket (*scenario b*). The purpose of these pictures is mainly qualitative to show the correct operation of the localization system. The solid lines represent the estimated trajectories, whereas the dashed lines refer to the routes reconstructed using the scanner data. The sporadic adjustments in position or orientation due to tag or marker detection

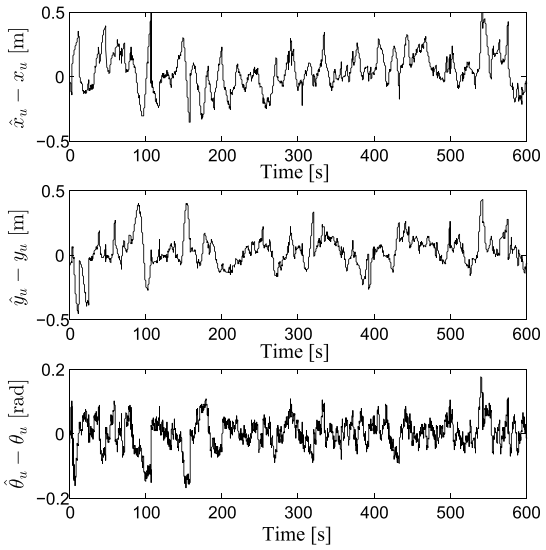


Fig. 7. Differences (as a function of time) between the values of $\hat{x}_u$, $\hat{y}_u$, and $\hat{\theta}$ estimated by the c-Walker positioning system and the corresponding values measured with the laser scanner during a 10-min long experiment.

are quite evident. At a glance, the positioning uncertainty is generally well below 50 cm and always smaller than 1 m.

Fig. 7 shows the differences between the values of $\hat{x}_u$, $\hat{y}_u$, and $\hat{\theta}$ estimated by the c-Walker positioning system and the corresponding values measured with the laser scanner during a travel of about 10 min in the empty room. The error patterns are not white, but the position uncertainty in $x$ and $y$ is generally well below $\pm 50$ cm even in the long run. Similar considerations also hold for the orientation uncertainty, which is generally bounded within $\pm 0.15$ rad, as expected. The most interesting outcome of this experiment is the substantial lack of drift phenomena.

Fig. 8(a)–(c) shows the histograms of the values of $\hat{x}_u - x_u$, $\hat{y}_u - y_u$, and $\hat{\theta} - \theta$, respectively, collected in seven further experiments. In each of them, the user continuously pushes the c-Walker in all directions for at least 350 s without meeting any obstacle. Due to the quite high sampling rate (i.e., 250 Hz), the total number of data is very large, in the order of $5 \times 10^5$ samples. Even if the estimated probability density functions seem to be Gaussian, a more careful analysis based on normal probability plots (not reported for the sake of brevity) shows that they are not. However, all distributions are quite symmetric with a mean value equal to 0 and standard deviations equal to 18 cm (for both $x_u$ and $y_u$) and 0.06 rad for $\theta$, respectively.

Finally, Table II summarizes the results of a more exhaustive characterization performed over a set of about 70 experiments of about 180 s each, with the walker moving in the room both with and without obstacles. The values in Table II are the median as well as the 75th, 95th, and 99th percentiles of the RMS position and orientation errors, respectively, in steady state. This is supposed to be reached after a few adjustments performed through RFID tag or marker detection. Like in Section V, the individual position error values are given by the Euclidean distance between the coordinates measured by

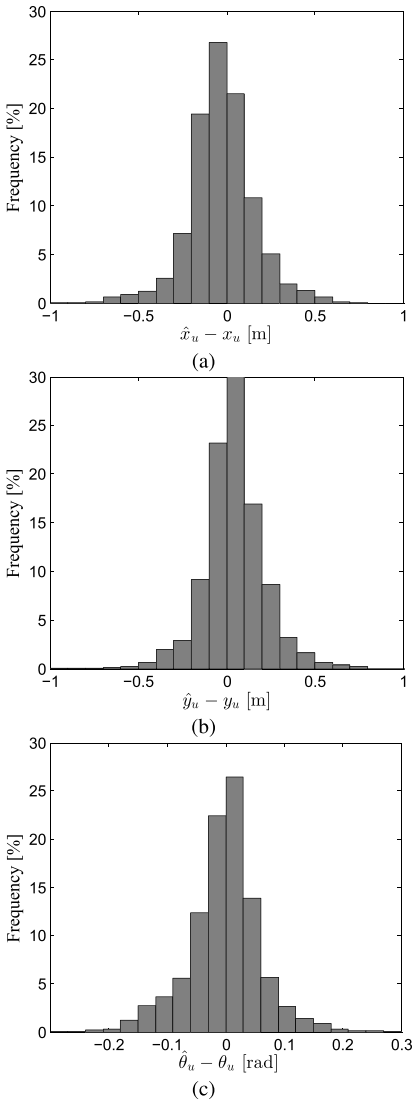


Fig. 8. Histograms of the values of (a) $\hat{x}_u - x_u$, (b) $\hat{y}_u - y_u$, and (c) $\hat{\theta} - \theta$ collected in seven experiments of at least 350 s each.

TABLE II
MEDIAN VALUE, AS WELL AS 75TH, 95TH, AND 99TH PERCENTILES OF THE RMS (EUCLIDEAN) POSITION AND ORIENTATION ERRORS IN STEADY-STATE CONDITIONS OVER ABOUT 70 DIFFERENT ROUTES OF 180 s EACH

| **Percentile [%]** | **50** | **75** | **95** | **99** |
|---|---|---|---|---|
| **RMS position error [cm]** | 40 | 45 | 50 | 75 |
| **RMS orientation error [rad]** | 0.10 | 0.11 | 0.14 | 0.17 |

the laser scanner at a given time and the estimated trajectory at the same time. It is worth noting that the 95th percentiles are compliant with the wanted specifications and with the results of the simulation-based design reported in Section V. In fact, the RMS position and orientation errors are smaller or equal to 50 cm and 0.15 rad, respectively, with at least 95% probability.

## VII. CONCLUSION

In this paper, a positioning algorithm for wheeled devices is presented and characterized experimentally. The proposed solution has been developed and implemented for a smart

walker assisting older adults to safely navigate in large and complex public environments. However, it can also be used with minor modifications in different contexts, e.g., robotics. The algorithm relies on odometry and multisensor data fusion, namely, on an EKF that estimates position and orientation, while compensating for the angular and forward velocity systematic drifts caused by possible asymmetries or differences between the left- or right-side encoders and wheels. Passive RFID tags and simple visual markers on the floor provide accurate and sporadic adjustments in position and orientation, respectively. A conservative criterion is described to minimize the number of such devices (or, dually, to maximize the distance between them), while keeping the position and orientation uncertainty within given boundaries. Compared with other RFID-based solutions, the proposed approach requires grids with a coarser granularity (i.e., less devices in the environment) and comparable performances (accuracy on the order a few tens of centimeters in the long run). Several experiments on the field confirm that the system meets such requirements with a high level of confidence.

## ACKNOWLEDGMENT

The authors would like to thank Prof. P. Macchi from the Center for Integrative Biology of the University of Trento, Prof. M. De Cecco from the Department of Industrial Engineering of the University of Trento, and Dr. M. Corrà from Tretec S.r.L., Trento, for their valuable support to the experimental activities described in this paper.

## REFERENCES

[1] *Indoor Location Market [Indoor Positioning and Indoor Navigation (IPIN); Indoor Mapping; Indoor LBS; Indoor Analytics; by Positioning Systems (Network-Based, Independent, Hybrid)]: Global Advancements, Market Forecasts and Analysis (2013–2018)*, Markets & Markets, 2013.

[2] S. Eisa and A. Moreira, "Requirements and metrics for location and tracking for ambient assisted living," in *Proc. Int. Conf. Indoor Positioning Indoor Navigat. (IPIN)*, Sydney, NSW, Australia, Nov. 2012, pp. 1–7.

[3] P. Pivato, L. Palopoli, and D. Petri, "Accuracy of RSS-based centroid localization algorithms in an indoor environment," *IEEE Trans. Instrum. Meas.*, vol. 60, no. 10, pp. 3451–3460, Oct. 2011.

[4] I. Neri, R. Centonze, M. L. Fravolini, and A. Moschitta, "A simple ranging technique based on received signal strength measurements in a narrowband 2.4 GHz channel: A space diversity approach," in *Proc. IEEE Int. Workshop Meas. Netw. (M&N)*, Naples, Italy, Oct. 2013, pp. 189–194.

[5] D. Han, S. Jung, M. Lee, and G. Yoon, "Building a practical Wi-Fi-based indoor navigation system," *IEEE Pervasive Comput.*, vol. 13, no. 2, pp. 72–79, Apr./Jun. 2014.

[6] M. A. Stelios, A. D. Nick, M. T. Effie, K. M. Dimitris, and S. C. A. Thomopoulos, "An indoor localization platform for ambient assisted living using UWB," in *Proc. 6th Int. Conf. Adv. Mobile Comput. Multimedia (MoMM)*, Nov. 2008, pp. 178–182.

[7] A. Cazzorla, G. de Angelis, A. Moschitta, M. Dionigi, F. Alimenti, and P. Carbone, "A 5.6-GHz UWB position measurement system," *IEEE Trans. Instrum. Meas.*, vol. 62, no. 3, pp. 675–683, Mar. 2013.

[8] C. Rohrig and M. Muller, "Localization of sensor nodes in a wireless sensor network using the nanoLOC TRX transceiver," in *Proc. IEEE 69th Veh. Technol. Conf. (VTC)*, Apr. 2009, pp. 1–5.

[9] H. Hur and H.-S. Ahn, "A circuit design for ranging measurement using chirp spread spectrum waveform," *IEEE Sensors J.*, vol. 10, no. 11, pp. 1774–1778, Nov. 2010.

[10] C. M. De Dominicis, P. Pivato, P. Ferrari, D. Macii, E. Sisinni, and A. Flammini, "Timestamping of IEEE 802.15.4a CSS signals for wireless ranging and time synchronization," *IEEE Trans. Instrum. Meas.*, vol. 62, no. 8, pp. 2286–2296, Aug. 2013.

[11] L. Angrisani, A. Baccigalupi, and R. Schiano Lo Moriello, "Ultrasonic time-of-flight estimation through unscented Kalman filter," *IEEE Trans. Instrum. Meas.*, vol. 55, no. 4, pp. 1077–1084, Aug. 2006.

[12] B. Andò, S. Baglio, and C. O. Lombardo, "RESIMA: An assistive paradigm to support weak people in indoor environments," *IEEE Trans. Instrum. Meas.*, vol. 63, no. 11, pp. 2522–2528, Nov. 2014.

[13] A. Bondavalli, F. Brancati, A. Ceccarelli, L. Falai, and M. Vadursi, "Resilient estimation of synchronisation uncertainty through software clocks," *Int. J. Critical Comput.-Based Syst.*, vol. 4, no. 4, pp. 301–322, Feb. 2013.

[14] E. Foxlin, "Pedestrian tracking with shoe-mounted inertial sensors," *IEEE Comput. Graph. Appl.*, vol. 25, no. 6, pp. 38–46, Nov./Dec. 2005.

[15] A. R. Jimenez, F. Seco, J. C. Prieto, and J. Guevara, "Indoor pedestrian navigation using an INS/EKF framework for yaw drift reduction and a foot-mounted IMU," in *Proc. 7th Workshop Positioning Navigat. Commun. (WPNC)*, Dresden, Germany, Mar. 2010, pp. 135–143.

[16] A. Colombo, D. Fontanelli, D. Macii, and L. Palopoli, "Flexible indoor localization and tracking based on a wearable platform and sensor data fusion," *IEEE Trans. Instrum. Meas.*, vol. 63, no. 4, pp. 864–876, Apr. 2014.

[17] R. Mautz and S. Tilch, "Survey of optical indoor positioning systems," in *Proc. Int. Conf. Indoor Positioning Indoor Navigat. (IPIN)*, Guimarães, Portugal, Sep. 2011, pp. 1–7.

[18] N. Conci, A. Armanini, M. Daldoss, A. Colombo, D. Fontanelli, and L. Palopoli, "Wireless sensor networks and video analysis for scalable people tracking," in *Proc. 5th Int. Symp. Commun., Control, Signal Process.*, Rome, Italy, May 2012, pp. 1–4.

[19] L. Klingbeil, M. Romanovas, P. Schneider, M. Traechtler, and Y. Manoli, "A modular and mobile system for indoor localization," in *Proc. Int. Conf. Indoor Positioning Indoor Navigat. (IPIN)*, Zürich, Switzerland, Sep. 2010, pp. 1–10.

[20] G. Panahandeh, M. Jansson, and S. Hutchinson, "IMU-camera data fusion: Horizontal plane observation with explicit outlier rejection," in *Proc. Int. Conf. Indoor Positioning Indoor Navigat. (IPIN)*, Montbeliard, France, Oct. 2013, pp. 1–9.

[21] P. Nazemzadeh, D. Fontanelli, D. Macii, and L. Palopoli, "Indoor positioning of wheeled devices for ambient assisted living: A case study," in *Proc. IEEE Int. Instrum. Meas. Technol. Conf. (I2MTC)*, Montevideo, Uruguay, May 2014, pp. 1421–1426.

[22] P. Nazemzadeh, D. Fontanelli, and D. Macii, "An indoor position tracking technique based on data fusion for ambient assisted living," in *Proc. IEEE Int. Conf. Comput. Intell. Virtual Environ. Meas. Syst. Appl. (CIVEMSA)*, Milan, Italy, Jul. 2013, pp. 7–12.

[23] P. Nazemzadeh, D. Fontanelli, D. Macii, T. Rizano, and L. Palopoli, "Design and performance analysis of an indoor position tracking technique for smart rollators," in *Proc. Int. Conf. Indoor Positioning Indoor Navigat. (IPIN)*, Montbeliard-Belfort, France, Oct. 2013, pp. 1–10.

[24] M. De Cecco, "Sensor fusion of inertial-odometric navigation as a function of the actual manoeuvres of autonomous guided vehicles," *Meas. Sci. Technol.*, vol. 14, no. 5, pp. 643–653, May 2003.

[25] S. Park and S. Hashimoto, "Autonomous mobile robot navigation using passive RFID in indoor environment," *IEEE Trans. Ind. Electron.*, vol. 56, no. 7, pp. 2366–2373, Jul. 2009.

[26] B.-S. Choi and J.-J. Lee, "Sensor network based localization algorithm using fusion sensor-agent for indoor service robot," *IEEE Trans. Consum. Electron.*, vol. 56, no. 3, pp. 1457–1465, Aug. 2010.

[27] B.-S. Choi, J.-W. Lee, J.-J. Lee, and K.-T. Park, "A hierarchical algorithm for indoor mobile robot localization using RFID sensor fusion," *IEEE Trans. Ind. Electron.*, vol. 58, no. 6, pp. 2226–2235, Jun. 2011.

[28] M. Y. Ahmad and A. S. Mohan, "Novel bridge-loop reader for positioning with HF RFID under sparse tag grid," *IEEE Trans. Ind. Electron.*, vol. 61, no. 1, pp. 555–566, Jan. 2014.

[29] V. Kulyukin, A. Kutiyanawala, E. LoPresti, J. Matthews, and R. Simpson, "iWalker: Toward a rollator-mounted wayfinding system for the elderly," in *Proc. IEEE Int. Conf. RFID*, Las Vegas, NV, USA, Apr. 2008, pp. 303–311.

[30] A. A. Nazari Shirehjini, A. Yassine, and S. Shirmohammadi, "An RFID-based position and orientation measurement system for mobile objects in intelligent environments," *IEEE Trans. Instrum. Meas.*, vol. 61, no. 6, pp. 1664–1675, Jun. 2012.

[31] P. Pivato, S. Dalpez, and D. Macii, "Performance evaluation of chirp spread spectrum ranging for indoor embedded navigation systems," in *Proc. IEEE Int. Symp. Ind. Embedded Syst. (SIES)*, Karlsruhe, Germany, Jun. 2012, pp. 307–310.

[32] H. A. Mallot, H. Bülthoff, J. J. Little, and S. Bohrer, "Inverse perspective mapping simplifies optical flow computation and obstacle detection," *Biol. Cybern.*, vol. 64, no. 3, pp. 177–185, Jan. 1991.
[33] Y. Bar-Shalom, X. Rong Li, and T. Kirubarajan, *Estimation With Application to Tracking and Navigation—Theory, Algorithm and Software*. New York, NY, USA: Wiley, 2001.

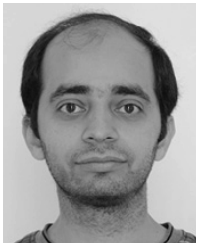

**Payam Nazemzadeh** (S'13) received the M.S. degree in mechatronics engineering from the University of Semnan, Semnan, Iran, in 2011. He is currently pursuing the Ph.D. degree in information and communication technology with the Department of Information Engineering and Computer Science, University of Trento, Trento, Italy.

He has been with the Department of Information Engineering and Computer Science, University of Trento, since 2012. He is a Visiting Researcher with the Department of Signal Processing, Royal Institute of Technology, Stockholm, Sweden. His current research interests include estimation theory, indoor localization, sensor data fusion, and automatic control.

**Federico Moro** received the B.S. and M.S. degrees in computer science and the Ph.D. degree in information and communication technologies from the University of Trento, Trento, Italy, in 2008, 2011, and 2015, respectively.

His current research interests include localization and control of robotic vehicles, and assisted living robotics.

**Daniele Fontanelli** (M'09) received the M.S. degree in information engineering and the Ph.D. degree in automation, robotics, and bioengineering from the University of Pisa, Pisa, Italy, in 2001 and 2006, respectively.

He was a Visiting Scientist with the Vision Laboratory, University of California at Los Angeles, Los Angeles, CA, USA, from 2006 to 2007. From 2007 to 2008, he had been an Associate Researcher with the Interdepartmental Research Center E. Piaggio, University of Pisa. From 2008 to 2013, he joined as an Associate Researcher with the Department of Information Engineering and Computer Science, University of Trento, Trento, Italy. Since 2014, he has been with the Department of Industrial Engineering, University of Trento. He has authored or co-authored over 70 scientific papers. His current research interests include real-time control and estimation, clock synchronization algorithms, resource aware control, visual servoing, localization algorithms, and service robotics.

**David Macii** (M'06–SM'14) received the M.S. degree in electronics engineering and the Ph.D. degree in information engineering from the University of Perugia, Perugia, Italy, in 2000 and 2003, respectively, and the master's degree in embedded system design from the Advanced Learning and Research Institute, University of Lugano, Lugano, Switzerland.

He was a Visiting Researcher at the Department of Electronic Systems, University of Westminster, London, U.K., in 2002, and the Advanced Learning and Research Institute, University of Lugano, from 2003 to 2005. From 2005 to 2012, he was an Assistant Professor with the Department of Information Engineering and Computer Science, University of Trento, Trento, Italy. From 2009 to 2010, he was with the Berkeley Wireless Research Center, University of California at Berkeley, Berkeley, CA, USA, as a Fulbright Research Scholar. He is currently an Associate Professor with the Department of Industrial Engineering, University of Trento. He has authored or co-authored about 100 papers in scientific journals and international conference proceedings. His current research interests include the development of measurement and estimation techniques based on digital signal processing for embedded systems.

**Luigi Palopoli** received the M.S. degree in computer engineering from the University of Pisa, Pisa, Italy, in 1998, and the Ph.D. degree in computer engineering from the Scuola Superiore Sant'Anna, Pisa, in 2002.

He is currently an Associate Professor with the Department of Information Engineering and Computer Science, University of Trento, Trento, Italy. His current research interests include embedded system design with a particular focus on real-time embedded control, formal methods, and stochastic analysis of real-time system.

Dr. Palopoli has served on the program committee of different conferences in real-time and control systems.